Investigation of control algorithm for long-stroke fast tool servo system

Zheng Gong[1], Dehong Huo[1*], Zengyuan Niu[2], Wanqun Chen[2], Islam Shyha[3]

[1]School of Engineering, Newcastle University, Newcastle upon Tyne, NE1 7RU, UK

[2]Uptech, Jiangsu Industrial Technology Research Institute, Kunshan, Jiangsu Province, China, 215300

[3]School of Engineering and the Built Environment, Edinburgh Napier University; Edinburgh EH10 5DT, UK

*Corresponding author. D. Huo, Tel.: +44 (0)1912086230 E-mail address: dehong.huo@newcastle.ac.uk

Abstract: Fast tool servo (FTS) is an efficient and reliable method in precision machining for fabricating freeform surfaces or microarrays with sub-micrometric form accuracy. In this paper, a Lorentz force FTS is designed where the voice coil motor is located inside the slide, and four air bearings are used as support components. Three different control algorithms, namely conventional PID control, advanced PID control with velocity/acceleration feed-forward (FF) and sliding mode control (SMC) are implemented in the system, and corresponding Simulink simulation models are built including for both mechanical and electrical systems. The results show that advanced PID and SMC can reduce phase error and overshoot, and tracking error can be controlled at 3.13% at 50 Hz. A new hybrid control algorithm (PID+SMC+FF) is developed, with system tracking error subsequently decreased to 0.871% at 50 Hz. In addition, with a suitable compensation method, the steady state tracking error is further decreased to 0.029%. Consistent results from testing with signals of different input frequency also indicate the general effectiveness of the algorithm.

Keywords: fast tool servo; PID control; feed-forward control; sliding mode control; tracking performance

1. Introduction

Fast tool servo (FTS) is an efficient technology for the manufacture of optical freeform or micro-structured surfaces [1-2]. Currently, piezoelectric (PZT) FTS and Lorentz force (LF) FTS systems have been developed for different shapes of surfaces. With well-designed flexure hinges and an appropriate power source for the piezoelectric ceramics, the PZT FTS system has high dynamic stiffness and can achieve high frequency responses up to several kHz and

achieve micrometric displacements [3-4]. Critical problems with the PZT-FTS involve the method used to control strong nonlinearity [3] and the design of the flexure hinge [4]. The latter's stiffness and coupling are the main design targets in the PZT-FTS mechanical design. Yang *et al.* [5] designed a PZT-FTS with a static stiffness of 33.62 N/μm and 20 μm stroke. Finite element analysis was adopted to get 2191 Hz dominant natural frequency. LF-FTS is usually driven by a voice coil motor and supported by air bearings. It can reach millimetre level displacements, but the range of response frequency is limited to tens or hundreds of Hertz [6]. Challenges associated with LF-FTS designs include inertia force [7], which causes the system to vibrate, and control of the undamped system [8].

For an FTS system, the use of high-frequency responses means that the system is sensitive to external disturbance and changes in internal factors [9], and thus it requires an effective control system and algorithm to ensure positional accuracy and tracking performance. The proportional integral derivative (PID) control algorithm is a classic and widely used algorithm. Wang *et al.* [10] used a closed-loop PI controller with feed-forward control in a PZT-FTS system (with a maximum amplitude of 10 μm), which reduced tracking error to less than 150nm. Lu *et al.* [11] combined a PI controller with a loop shaping compensator and adaptive feed-forward cancellation for a fast tool servo system driven by an ultrafast motor. The tracking error was 2.1nm (0.04%) when tracking a 16 μm @ 3 kHz sinusoid signal. Wang and Yang [12] used a PID controller with plug-in repetitive control for a PZT-FTS system designed for non-circular piston turning, and the system achieved a tracking error of 5 μm (less than 1%). For some FTS systems, combinations of PID controllers with other advanced algorithms such as feed-forward, adaptive or repetitive control can achieve even better tracking performance. However, the PID control algorithm has an overshoot problem and the parameters cannot be changed in real-time.

Apart from PID control, other algorithms are also implemented in FTS systems. Ma *et al.* [13] added repetitive control to a PZT-FTS system with a PI + feed-forward controller. Tracking error was reduced to 3 μm after tens of periods when tracking a sinusoidal signal of 0.4 mm @ 100 Hz. Adaptive control can be considered an improved algorithmic method of repetitive control. Zhou *et al.* [14] developed a novel adaptive feed-forward cancellation (AFC) control which can ameliorate the overshoot problem and improve tracking performance by about 2 orders of magnitudes. Robustness to frequency variations was also verified. Meanwhile, in active disturbance rejection control (ADRC) a state observer is built to deal with external disturbance in the FTS system which can decrease the side-effects caused by unknown

disturbance [15]. Wu *et al.* [16] designed an ADRC algorithm with feed-forward error compensation for a LF-FTS system. Actual machining tests were carried out and the tracking error was found to be less than 2 μm at cutting depths less than 0.4 mm. With the development of FTS algorithms, some advanced control methods such as zero phase error tracking (ZPETC) and sliding mode control (SMC) have been introduced which can be used to solve specific problems like phase error or overshoot in these control systems.

Lin and Chen [17] presented double feed-forward compensation control for an XY piezo stage in which the algorithm was combined with PID, repetitive, and feed-forward control. Average errors of 0.0215 μm and 0.02 μm were detected for the X and Y axes respectively at 100 Hz, and no obvious phase errors were detected. Duan *et al.* [18] developed sliding mode repetitive control with feed-forward control, and tested 20 Hz, 50 Hz, 100 Hz and 200 Hz input signals in the designed system. Compared to PID control, the maximum tracking error was reduced from 10.92% to 0.82%.

ZPETC or feed-forward control can also predict the phase delay of the system, and these control algorithms have been combined with other control algorithms. Azzaro and Veiga [19] introduced a sliding mode controller based on neural networks, which were suitable for the single and output system. Zhang *et al.* [20] designed an SMC algorithm with a variable structure employing a new approaching law for a PZT-FTS, and system state error was reduced from 2% to 0.5% and the rise time was also reduced to 0.8ms. Moreover, the results showed that the system had the ability to deal with changes in the manufacturing processes used. SMC does not require the full specification of the system and furthermore is effective in resisting external disturbances. Hence it is suitable for nonlinear systems such as an FTS system, given a well-designed approaching law. But the problem of chatting may occur, which needs to be prevented when adopting an SMC algorithm.

Overall, there are many different control algorithms which have been developed and implemented with PZT-FTS. But evaluations of control algorithms for LF-FTS are lacking, and the influence of different control algorithms and parameters on system performance requires further analysis.

In this paper, an LF-FTS system is designed and built based on a voice coil motor and air bearings. The physical model and a corresponding simulation model are built. Three different control algorithms, namely PID, advanced PID and SMC are tested for the LF-FTS system. By combining the characteristics of three control algorithms, a new hybrid control algorithm is

designed and implemented for the LF-FTS system. The performance of each control algorithm includes the testing of step response, sine tracking performance and system bandwidth.

2. Design of the fast tool servo mechanical subsystem

2.1 Principle of FTS motion

The motion of an FTS is considered as a reciprocating motion in choosing a suitable driving source, where the motion can be described as:

$$X = f(t) \quad [1]$$

where X is the travel distance of the FTS system which is a function of time *t*. It can also be considered in terms of the movement locus of the system. All reciprocating movements can be described as the superposition of several trigonometric functions. Therefore, Equation [1] can be expanded to:

$$X = f(t) = A_0 + \sum_{i=1}^{n} Asin\,(\omega_i t + \varphi_i) \quad [2]$$

where the system motion is considered to be sinusoidal, and it is assumed that the displacement-time equation of the fast tool servo is:

$$X = Asin(\omega t) = Asin\,(2\pi f t) \quad [3]$$

$$v = \dot{X} = \omega A cos(\omega t) \quad [4]$$

$$a = \ddot{X} = -\omega^2 Asin\,(\omega t) \quad [5]$$

$$F = ma = -m\omega^2 Asin\,(\omega t) \quad [6]$$

where:

X is the travel distance of the system (m);

v is its speed (m/s);

a is acceleration (m/s^2);

t is time (s);

A is the maximum stroke (m);

f is the frequency (Hz);

ω is the angular frequency (rad/s);

F is the driving force (N); and

m is the mass of all the moving components (Kg).

In this paper, the maximum frequency is 100 Hz and the maximum stroke is 3mm, the total moving mass is no more than 1 Kg so that, according to Equation [6], the driving force should be greater than 60 N. The tracking error requirement is set as 5% when doing the rough tuning. And the ideal tracking error should be less than 1% when the fine-tuning is finished.

2.2 Mechanical structure of the FTS

To meet the system requirements, a voice coil motor (VCM) is chosen as the driving source. Its mass is 190.5 g and it can generate a continuous motor force of 64.6 N and a maximum stroke of 12.7 mm. A hollow square slide made of aluminium is designed as the guide mechanism with a mass of 721g. Four air bearings are designed as the support mechanism which gives negligible friction. A connection plate is used to connect the motor coil and the slide, and the four air bearings are located around the latter. The tool holder is located in the middle of the connection plate. The maximum stroke is limited by the bumper pads to ± 3 mm. A section view and schematic drawing of the FTS system are shown in Figure 1.

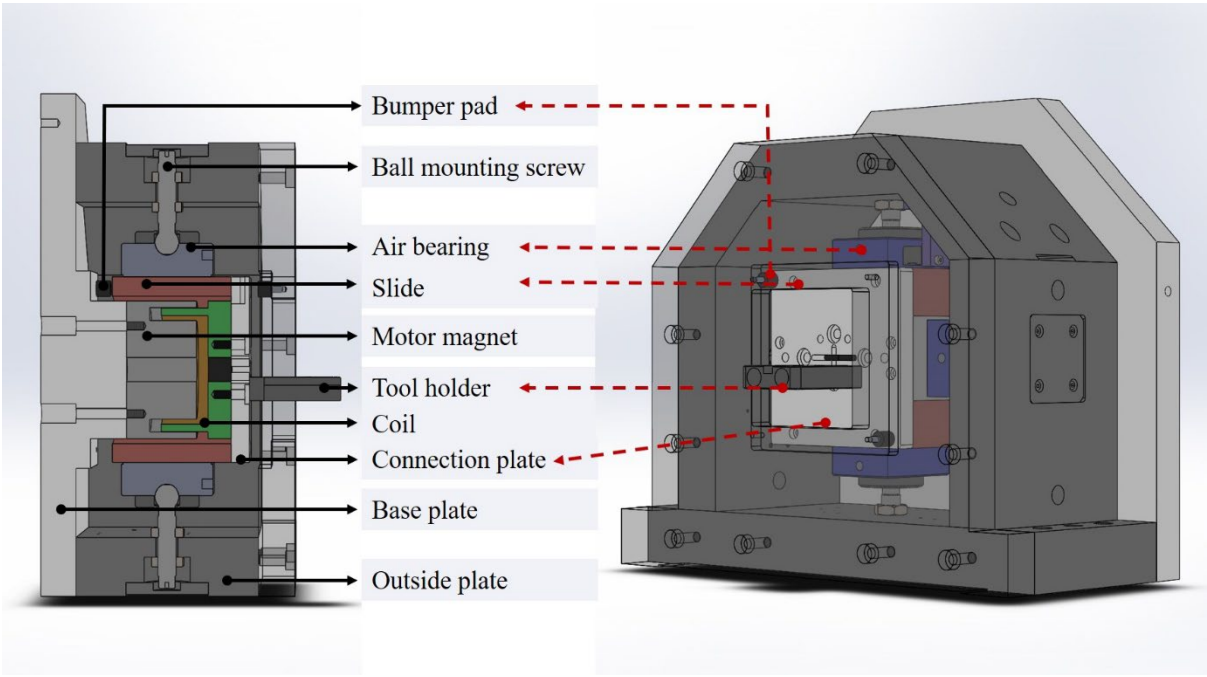

Figure 1 Section-view of the FTS system

Modal analysis is performed on the mechanical system, and the results show that the 1st order natural frequency is more than 328 Hz which is much higher than the intended working frequency of 100Hz, indicating that the mechanical design is suitable for this FTS system.

3. Design of the fast tool servo control subsystem

3.1 Hardware implementation

The LF-FTS control system includes a multi-axis precision motion controller (Omron CK3M) and a motor drive (Elmo Gold Hornet). The DSP controller CK3M was chosen because it allows user-defined control algorithms to be implemented. A high resolution optical linear encoder (Renishaw) is used as feedback element to form the positional closed loop. The system also comprises a current loop in the motor drive. The controller generates the desired signal in the form of analogue signals (±10 V) which are transferred to the motor drive which functions as the current loop, and it can enlarge the current on a certain scale and maintain the current signal in a stable state so as to prevent current overshoot. The signal is then transferred to the voice coil motor. Movements are detected by the linear encoder which generates the position signal back to the controller. A block diagram of the control system is shown in Figure 3.

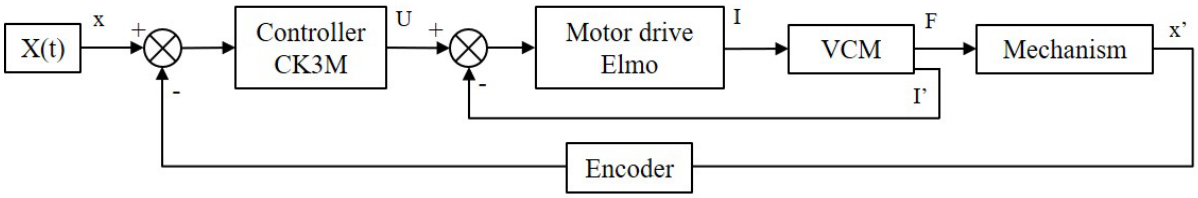

Figure 2 Control block diagram

The encoder in this paper generates a digital signal with 1 motor unit (mu) corresponding to 10 nm (1 mu = 10 nm). Therefore, the feedback can be considered to be linear. For example, for a system with a servo frequency of 16 kHz, if the desired motion signal is ±1 mm @ 30 Hz then the controller will generate a sine signal of 100000 mu @ 30 Hz. The controller will calculate this digital signal according to the position loop control algorithms and transform it into voltage signals. The motor drive amplifies the voltage signal, and can be considered as a PI controller for the current loop. In this research, a self-tuning function of the motor drive is adopted. The final bandwidth of the current loop is 3KHz, which is sufficient for the fast tool servo system. When the motor receives the current signal from the motor drive, it generates a motor force which carries the load to perform the desired motion. The system setup is shown

in Figure 3. All the following tests are based on the setup and the position signals are collected from the encoder feedback.

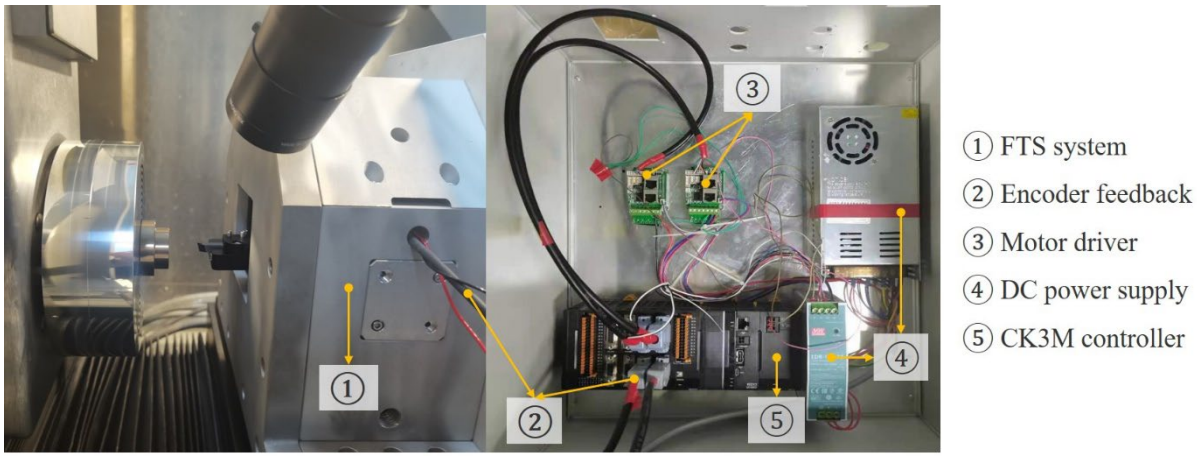

Figure 3 System setup

3.2 System identification and modelling

An open-loop frequency sweep from 0 Hz - 100 Hz is performed to conduct the system identification. The identification model is built and includes the current loop and the FTS mechanical system as shown in Figure 4. The controller generates the frequency sweep signal and feeds it to the system whose output displacement is recorded and transformed to the system velocity by the controller.

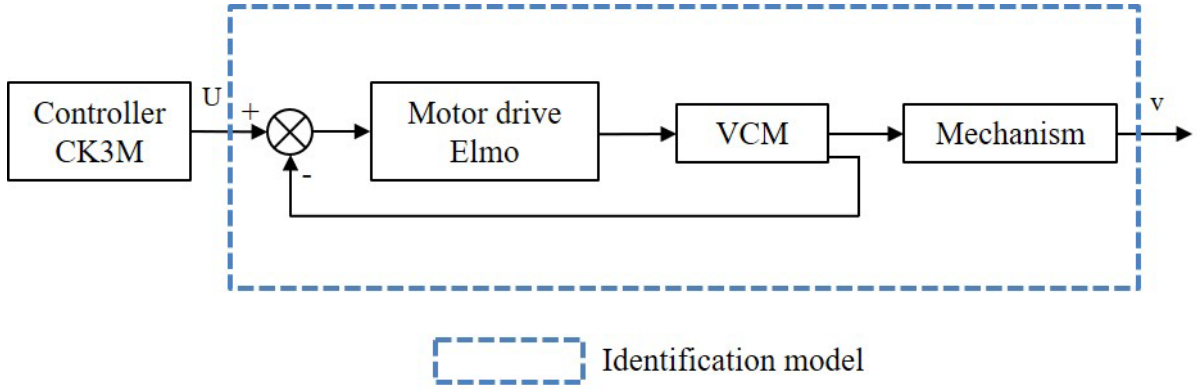

Figure 4 Schematic diagram of system identification

It should be noted that the controller output is ±10 V, whilst in the controller it is in the form of ±32768 digital signals according to 16 bits controller resolution. To render the identification model close to the physical model, no unit conversions are adopted here, and the open-loop frequency sweep results are shown in Figure 5.

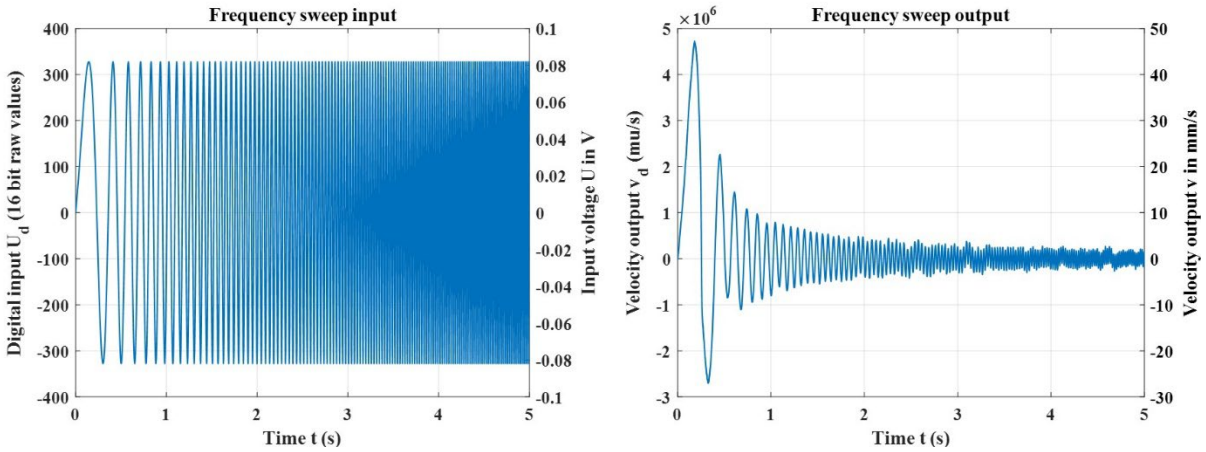

Figure 5 Input and output signals in open-loop frequency sweep

The state-space system identification model is used for the identification, as shown in Equation [7]. When the model number is 1, the fit to the estimated data reaches 99.31%.

$$\begin{cases} dx/dt = A\,x(t) + B\,u(t) + K\,e(t) \\ y(t) = C\,x(t) + D\,u(t) + e(t) \end{cases} \quad [7]$$

In the equation:

$A=11.37$, $B=0.0006759$, $C=2.293\times10^{8}$, $D=0$, $K=3.877\times10^{-5}$;

where K is a small number and $e(t)$ represents disturbances in the system. In the research, the influence of disturbances on the system is neglected. Next, the identification model is used to build a simulation model of the FTS system.

Since the output of the identification model is system velocity, an integrator is needed in the simulation model to transform velocity into a displacement signal. The control block diagram of the simulation model is shown in Figure 6.

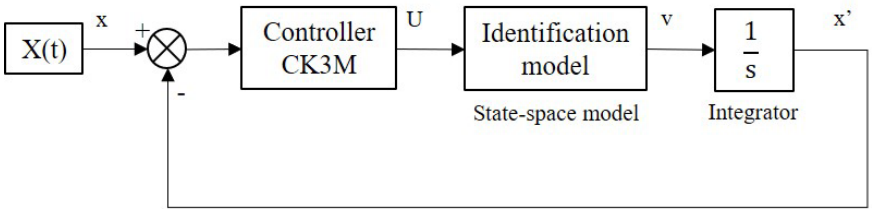

Figure 5 Control block diagram of the simulation model

To test the accuracy of the simulation model, the results are compared with physical test results. A simulation model is considered to be the ideal situation, but the real physical testing is a complex situation, with external disturbances such as electromagnetic interference and vibration affecting the results. Therefore, the output signal of the controller (U) is chosen for

comparison. If the controller output in the physical test and simulation model is in good agreement, then the simulation model can be deemed to be a good representation of the system. Also, the accuracy of the simulation model is the basis of the further development of control algorithms. An accurate simulation model can decrease the adjustment time when running the system physically, and the control parameters in the simulation model thereby allow a quicker start for the physical model. In addition, in the accuracy test, the control algorithm is the standard servo algorithm in the controller. The control parameters used in the simulation model and physical test are exactly the same and the same input signals of 30 and 50 Hz are generated in the simulation and physical models. The controller output is transformed into an analogue signal so that comparison is more straightforward.

Figure 7 and Figure 8 show the output of the controller from the simulation and physical tests with the same input signals of 30 and 50 Hz respectively. It can be seen that the results are in good agreement with an overall discrepancy below 2%. This confirms that the simulation model can accurately represent the actual system. Hence the simulation model is suitable for use in for control algorithm development.

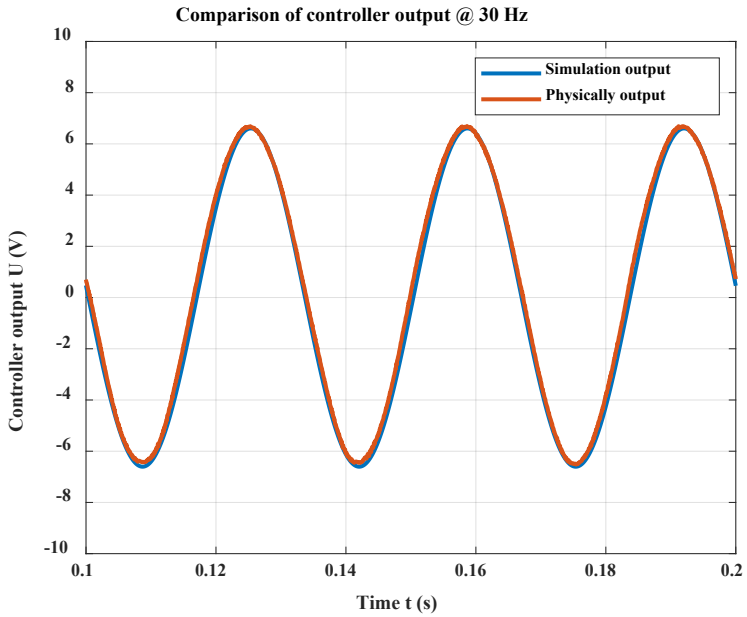

Figure 6 Comparison results of controller output @ 30 Hz

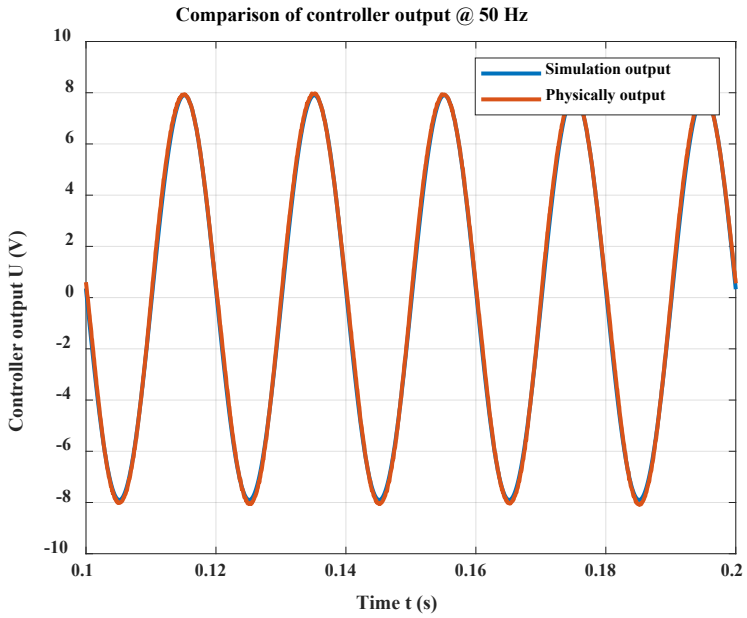

Figure 7 Comparison results of controller output @ 50 Hz

3.3 Control algorithms implementation and comparison

Three different control algorithms are implemented and compared in this research, namely PID, advanced PID control with velocity/acceleration feed-forward, and sliding mode control. For the convenience of explanation, the meanings of different signals are summarized in Table 1.

Table 1 Meanings of different signals

Name	Meaning	Value
CP(k)	Command position	From controller
AP(k)	Actual position	From encoder
CV(k)	Command velocity	CP(k)-CP(k-1)
CA(k)	Command acceleration	CV(k)-CV(k-1)
AV(k)	Actual velocity	AP(k)-AP(k-1)
e(k)	Tracking error	CP(k)-AP(k-1)

PID control is a classic control algorithm. It uses the error signal itself, and the integration and differentiation of the error signal to form the control law. The control law and block diagram are shown in Equation [8] and Figure 9 respectively.

$$u(k)_{PID} = K_p e(k) + K_i \sum_{j=0}^{k} e(j) + K_d[e(k) - e(k-1)] \quad [8]$$

where:

u(k) is the controller output;

K_p is the proportional gain;

K_i is the integration gain; and

K_d is the differentiation gain.

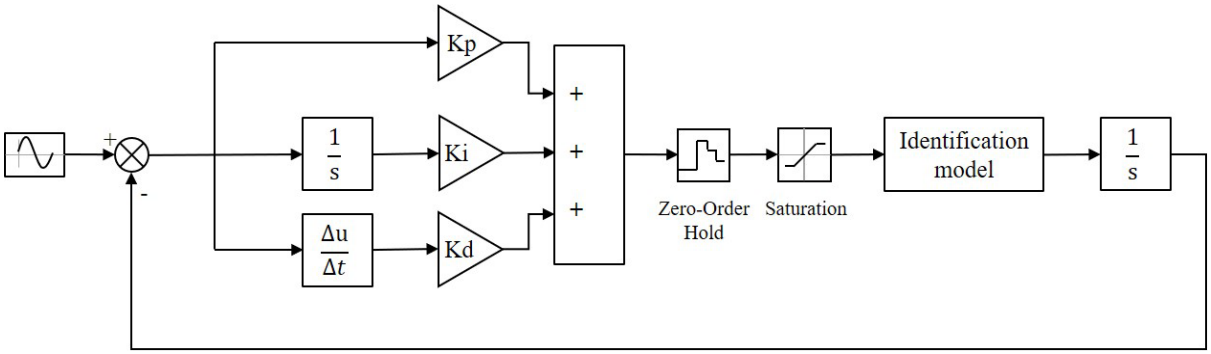

Figure 8 Control block diagram of PID control

The control block diagram is built to simulate the real output of the controller, so the zero-order hold transforms the continuous system into a discrete system, the sampling time is 0.0625 ms which corresponds to the frequency of the servo system of 16 kHz. The saturation block represents the limits of the controller output (±10 V).

The second control algorithm combines PID control and velocity/acceleration feed-forward control. The control law and block diagram are described in Equation [9] and Figure 10 respectively.

$$u(k)_{A\_PID} = K_p\left[e(k) + K_i \sum_{j=0}^{k} e(j)\right] + \left[K_{vff} CV(k) + K_{aff} CA(k)\right] - [K_{vfb} AV(k)] \quad [9]$$

where:

K_p is the proportional gain;

K_i is the integration gain;

K_{vfb} is the differentiation gain;

K_{vff} is the velocity feedforward gain; and

K_{aff} is the acceleration feedforward gain.

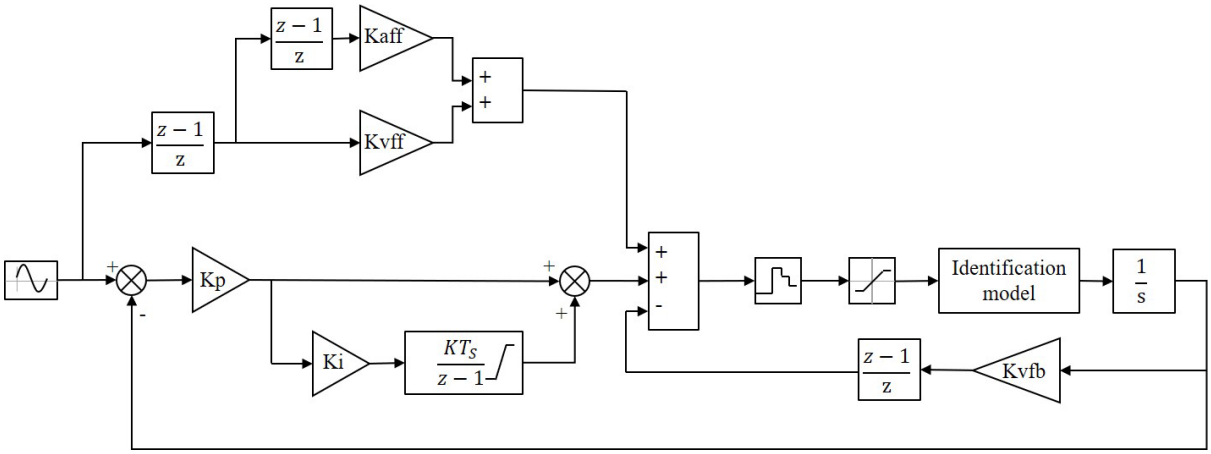

Figure 9 Control block diagram of Advanced PID control

K_p is used to offer sufficient control of the stiffness of the system. An increase in K_p can increase the response speed of the system; K_i is used to reduce the system's steady state error; K_{vfb} connects with the damping of the control system where, unlike in classic PID control, the differentiation gain takes effect on the actual position signal rather than the tracking error signal; K_{vff} can be set as equal to K_{vfb} in this application, and it is used to reduce the error caused by the overlarge differentiation gain. A suitable value of K_{aff} can reduce the inertia error of the system, especially for an FTS system where inertia force is directly proportional to the square of the frequency.

The final control algorithm is sliding mode control (SMC), which is a kind of nonlinear and discontinuous control. It is different from other traditional control algorithms in that SMC can change the control status of the object to be controlled according to its dynamic condition, thereby forcing the object to move along an as-designed track in what is called 'sliding mode'. The design of the SMC algorithm does not rely on the parameters and disturbance conditions of the control object; thus, the controller can respond more quickly. The key to the application of SMC is to choose a sliding mode surface (S) and build a suitably designed control law. In this paper, a second-order sliding mode surface is designed and the control law is designed in the form of a power series described in Equations [10] and [11]:

$$S = K_1 e(k) + K_2(e(k) - e(k-1)) \quad [10]$$

$$u(k)_{smc} = K_3 S + \sum_{j=0}^{k}(K_4 \cdot sign(S) \cdot |e(k)|) \quad [11]$$

where:

K_1 *and* K_2 are the sliding surface parameters;

K_3 *and* K_4 are the control law parameters; and

sign() is the sign function.

The control block diagram of the SMC is shown in Figure 11.

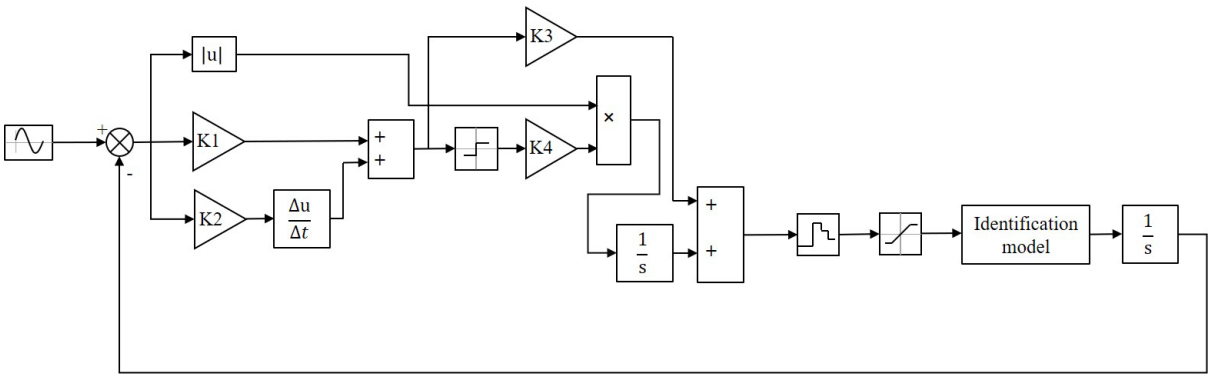

Figure 10 Control block diagram of SMC

In SMC, the stiffness and damping of the system are dependent on the parameters of the sliding surface. An increase in K_1 can increase the system control stiffness and response speed. System damping can be altered by adjusting K_2. At a logic combination of K_1 and K_2, the system can achieve suitable dynamic performance, while K_3 and K_4 are used to fine-tune the system. When it reaches acceptable dynamic performance, adjustments to K_3 and K_4 can decrease the phase error of the final system.

All three control algorithms are tested in the simulation and physical models. It should be noted that the simulation model represents the ideal running conditions of the FTS system, where there are no limitations on the control parameters which could cause the output of the controller to remain at the maximum value or chattering problems, shown in Figure 12.

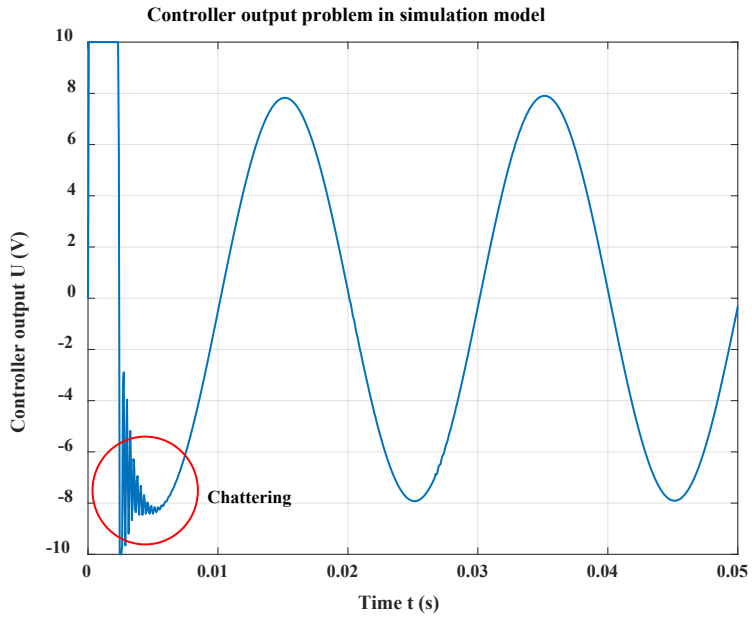

Figure 11 Controller output problem in simulation model

In the simulation model, the chattering of the controller output (red circle) does not affect the final performance. But in the physical model, the controller cannot realize this kind of high-frequency change. This will lead to the generation of controller noise and system vibration. Furthermore, divergence among the control algorithms could occur which would cause the failure of the whole system. Therefore, when adjusting the simulation model, system tracking performance is not the only index to focus on. The controller output signal is also important in the successful implementation of control algorithms.

After the simulation stage, the control algorithms with adjusted control parameters are written in the controller, and step response and system tracking performance tests are carried out on the physical model.

3.4 Performance of the control algorithms

A 1mm step signal is adapted to test the step response of the system with different control algorithms. The results are shown in Figure 13:

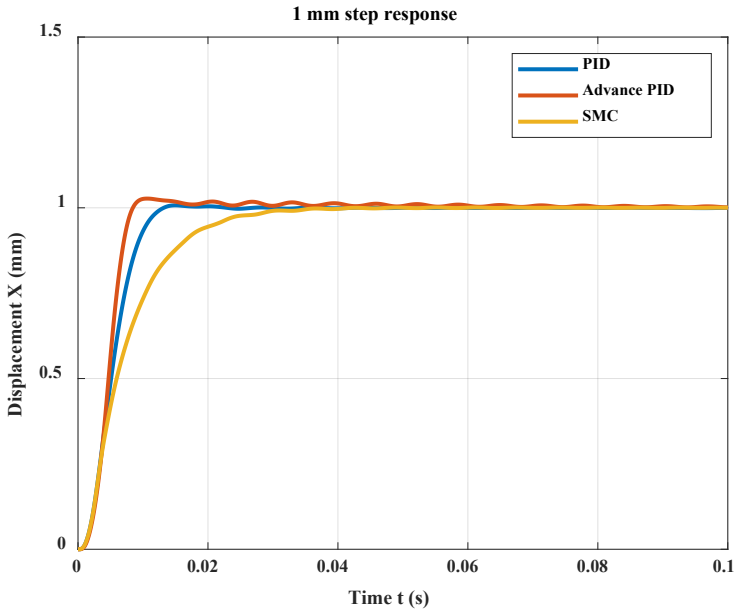

Figure 12 Step response of three different control algorithms

From the step response, the rise time and overshoot can be calculated, as shown in Table 2:

Table 2 Step response results of three control algorithms

Control algorithm	Rise time (s)	Overshoot

PID	0.012	0.68%
Advanced PID	0.014	2.70%
SMC	0.027	0.00%

The PID and advanced PID control enable the system to have a shorter response time, but overshoot also exists. The SMC solves the overshoot problem but the system needs more time to reach the command position. Overshoot could cause phase errors, whereas the longer rise time could also lead to phase errors while tracking the sine signal.

Four different sine signals were tested for the system, which are 1 mm @ 30 Hz; 0.68 mm @ 40 Hz; 0.43 mm @ 50 Hz; 0.3 mm @ 60 Hz. In the following discussion, 0.43 mm @ 50 Hz is chosen as an example to show the control algorithm's performances. Four indices can be calculated from the test results to represent signal tacking performances: the root-mean-square (RMS) error, steady-state error, amplitude difference and phase difference. Figure 14 (a) (b) and Equation [12] - [15] show the calculation steps for the four indices. Besides, All the values are given relatively to the input in the following calculation and comparisons.

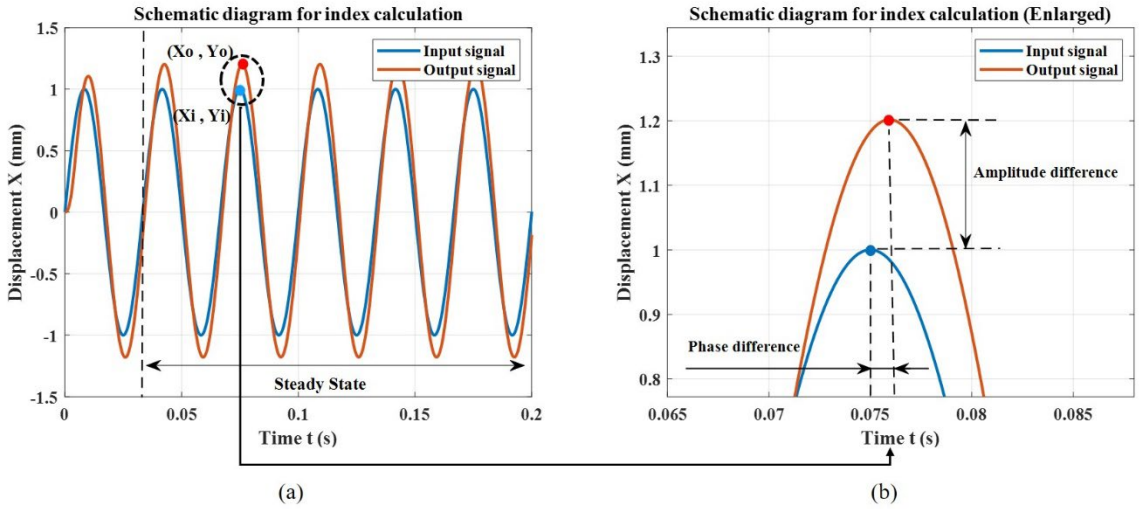

Figure 13 (a) (b) Schematic diagram for index calculations

$$RMS\ error = \frac{max\left(\sqrt{\frac{\sum_{k=1}^{N}(Output - Input)}{N}}\right)}{max\ (Input)} \quad [12]$$

$$Steady\ state\ error = \frac{max\ (Output - Input)}{max\ (Input)} \quad [13]$$

$$Amplitude\ difference = \frac{Yo - Yi}{Yi} \quad [14]$$

$$Phase\ difference = \frac{Xo - Xi}{Xi} \quad [15]$$

The tracking performance with PID control is shown in Figure 15.

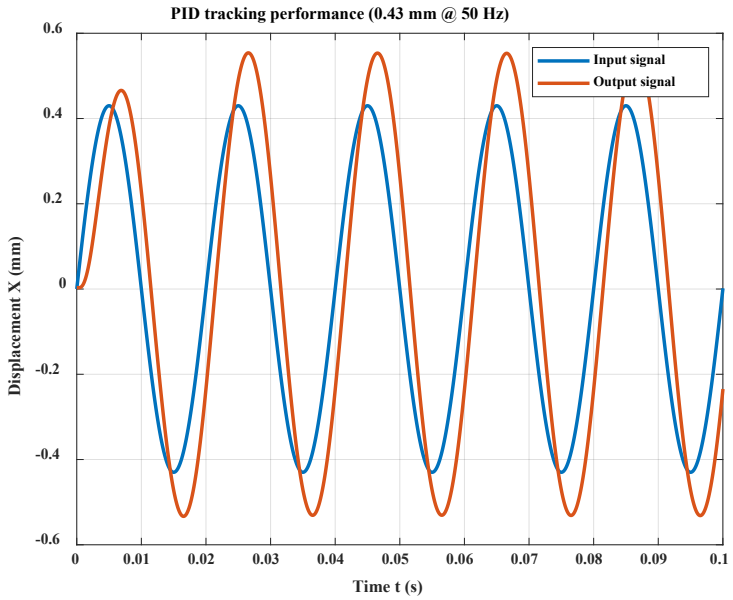

Figure 14 PID control sine signal tracking performance

The root-mean-square error and steady-state error of PID tracking performance are 51.387% and 75.034% respectively. The amplitude and phase errors are calculated from the peak points of the input and output signals, which give phase delays of 28.713% and 3.333% respectively.

The tracking performance with advanced PID control is shown in Figure 16.

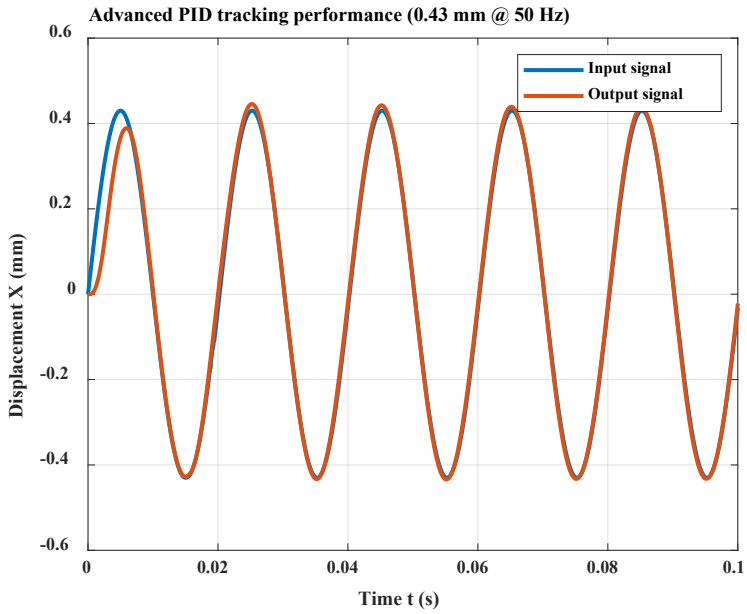

Figure 15 Advanced PID control sine signal tracking performance

The advanced PID control has an RMS error of 2.405%, 3.135% steady-state error and 2.939% phase error. No phase error is observed from the test results. Compared to PID control, the tracking performance has improved significantly, indicating that the addition of velocity/acceleration feed-forward control solves the phase error but overshoot still remains.

The tracking performance with SMC is shown in Figure 17.

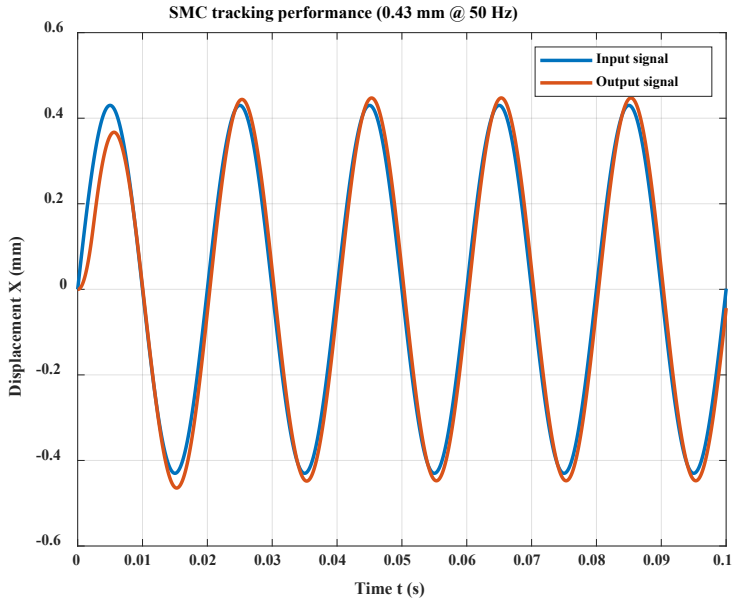

Figure 16 SMC sine signal tracking performance

The values of RMS and steady state error of SMC are 7.683% and 11.341% respectively; and the amplitude and phase errors are 5.209% and 0.691% phase delay respectively. The sine signal tracking performance of SMC is better than PID control but worse than the advanced PID control.

The tracking error curves of all three control algorithms are shown in Figure 18.

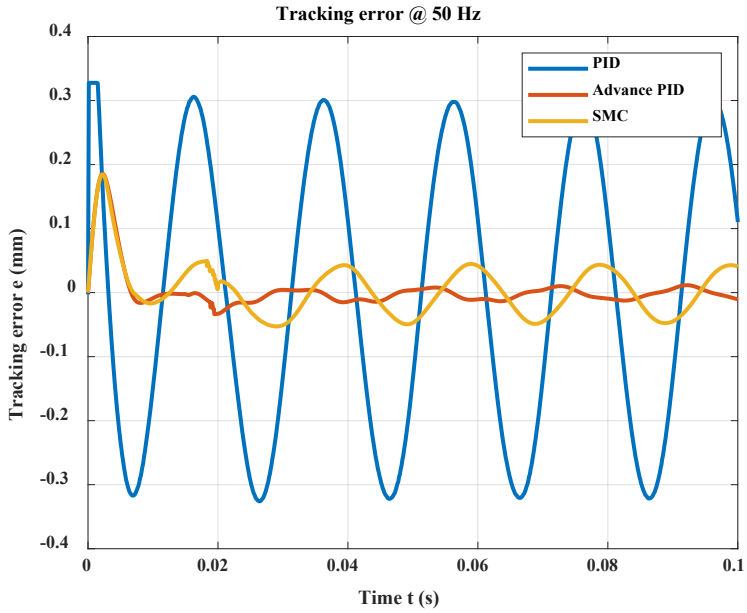

Figure 17 Tracking error of three control algorithms

When the system reaches the steady state, the tracking error is ±0.31 mm for PID control, ±0.012 mm for advanced PID control, and ±0.047 mm for the SMC algorithm. Also, for 50 Hz input, when the time is a multiple of 0.02 s, the tracking error at that time can represent the phase error because the ideal value should be 0, while a large value at that time reflects a large phase error. From Figure 18, it is obvious that the advanced PID control has the smallest phase error.

Among all the performance indices, steady state-error is most important. The primary goal of the control algorithm is to reduce the system's steady-state error to within an acceptable range. Then, the amplitude and phase errors can be used to build compensation for the system at the final stage in order to improve system performance further. To meet the requirement of high positional accuracy, the tracking steady-state error of the FTS system should as small as possible. The values of steady state error for different control algorithms with different input signals are summarised in Table 3.

Table 3 Steady state tracking errors of different control algorithms

Steady state error (e)				
	1.00 mm @ 30 Hz	0.68 mm @ 40 Hz	0.43 mm @ 50 Hz	0.3 mm @ 60 Hz
PID	25.702%	47.645%	75.034%	105.671%
Advanced PID	1.211%	1.938%	3.135%	5.560%
SMC	5.685%	8.411%	11.341%	14.286%

The steady-state error increases with the frequency of the input signal. When the command signal frequency reaches the maximum bandwidth of the system, it becomes difficult for the system to track it. The advanced PID control has the best performance among all the control algorithms in terms of steady-state error, but the value of the latter at the higher input frequency (>50Hz) also exceeds the requirement of 5% or less of this type of error.

Three typical control algorithms are designed and compared. For the application of FTS, advanced PID control can solve the phase error problem and SMC can solve the overshoot problem, but the steady error at high frequency is still high. Therefore, in order to achieve a higher tracking accuracy for the system, a hybrid control algorithm was designed for the FTS system.

4. Proposal of a hybrid control algorithm for the FTS system

4.1 Hybrid control algorithm design and tests

As discussed in Section 3, feed-forward control can eliminate phase error and SMC can reduce the overshoot. A hybrid control algorithm combining PID control, velocity/acceleration feed-forward (FF) control and SMC is proposed and its performance is discussed in this section. Figure 19 shows the control block diagram.

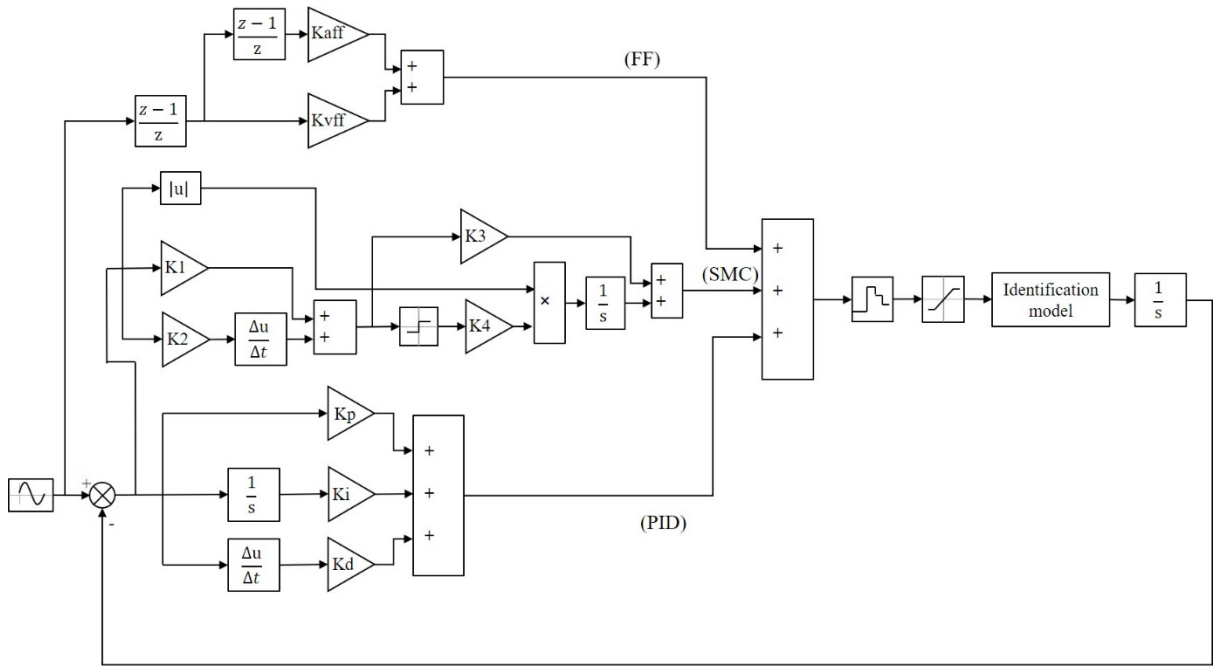

Figure 18 Control block diagram of new control algorithm for FTS system

Simulations were carried out to investigate the different combinations and influence of the PID+SMC+FF control algorithms on the FTS system. The tracking performance of different combinations is shown in Figure 20.

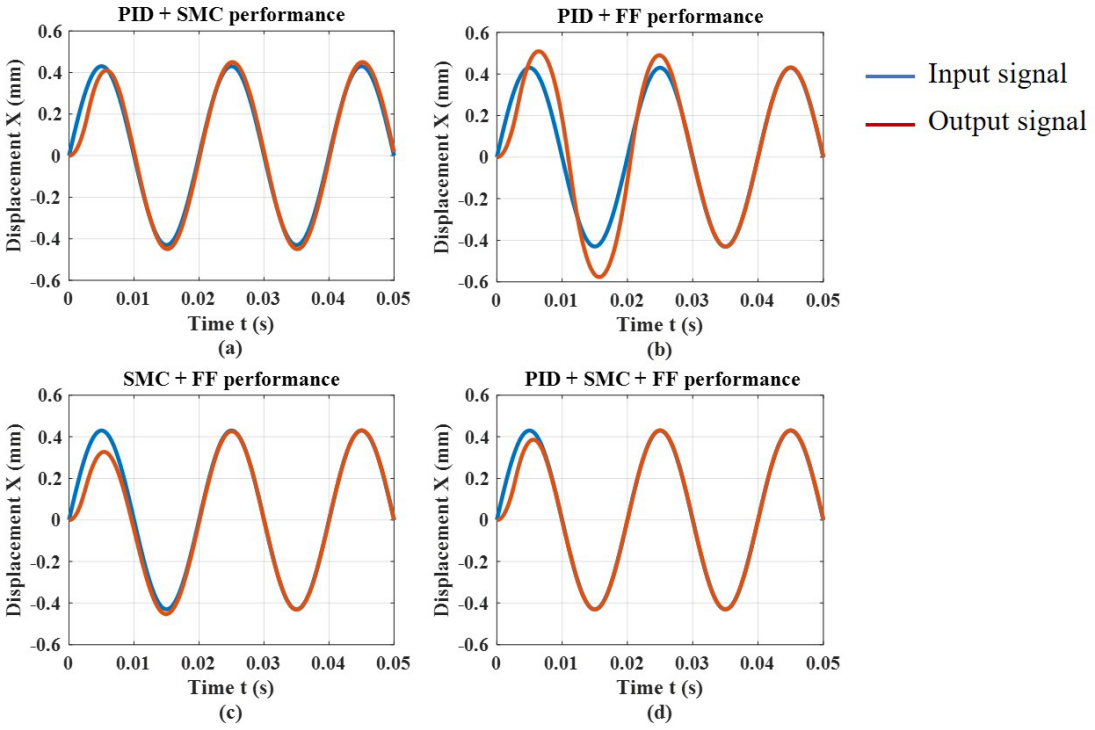

Figure 19 Sine signal tracking performance of different combinations:

(a) PID + SMC; (b) PID + FF; (c) SMC+FF, (d) PID+SMC+FF

Figure 20 shows the effectiveness of the PID+SMC+FF algorithms. It can be seen that the PID+SMC and SMC+FF algorithms can track the input sine signal, but their performance is not good enough, which is similar to the advanced control algorithm. The PID+FF algorithm shows good performance at the steady state, but the overshoot problem and phase error problems are significant in the first two periods, which could cause divergence in the physical model. Therefore, the combination of the three algorithms can give the system good sine signal tracking performance. After adjusting the control parameters in the simulation model, the control algorithm was written in the controller and some physical tests were carried out.

The 1mm step response results are shown in Figure 21.

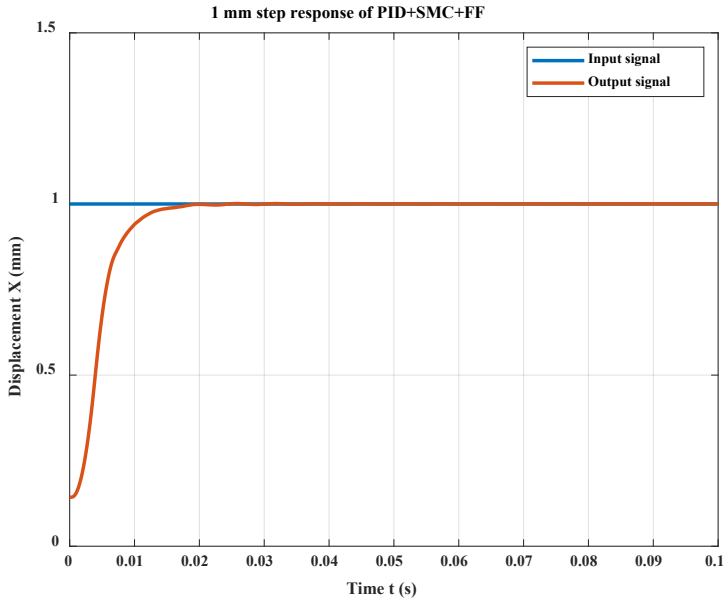

Figure 20 Step response of PID+SMC+FF

The rise time is 0.0134 s and the overshoot is 0.00%. The problem of overshoot is solved and the rise time is not extended. The sine signal tracking performance is shown in Figure 22.

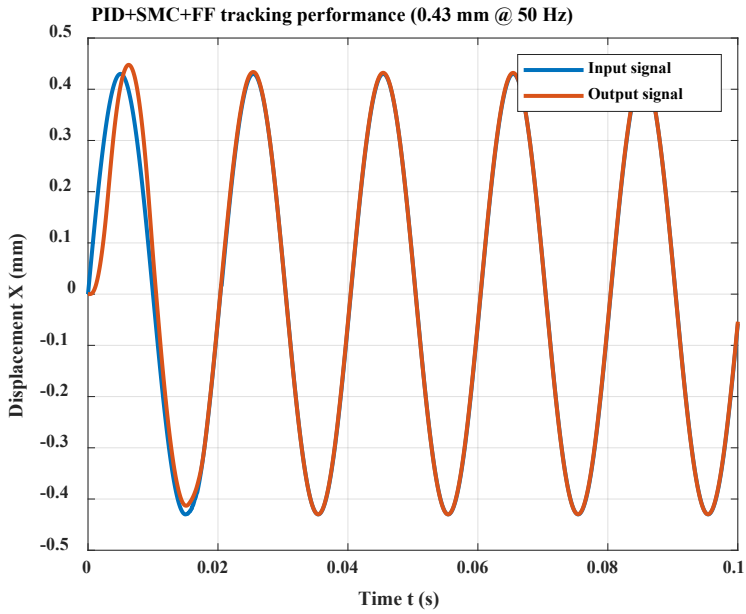

Figure 21 Sine signal tracking performance of PID+SMC+FF

The values of RMS and steady-state error are 1.954% and 0.871% respectively. The amplitude error is 0.447% and there are no phase errors. It can be seen in Figure 22 that the system reaches steady state after the first period and the output signal is close to the input signal.

According to section 3, the system with the advanced PID control algorithm gives the best tracking performances, and so the tracking error of the systems with advanced PID control and the hybrid control algorithm was compared. The results are shown in Figure 23.

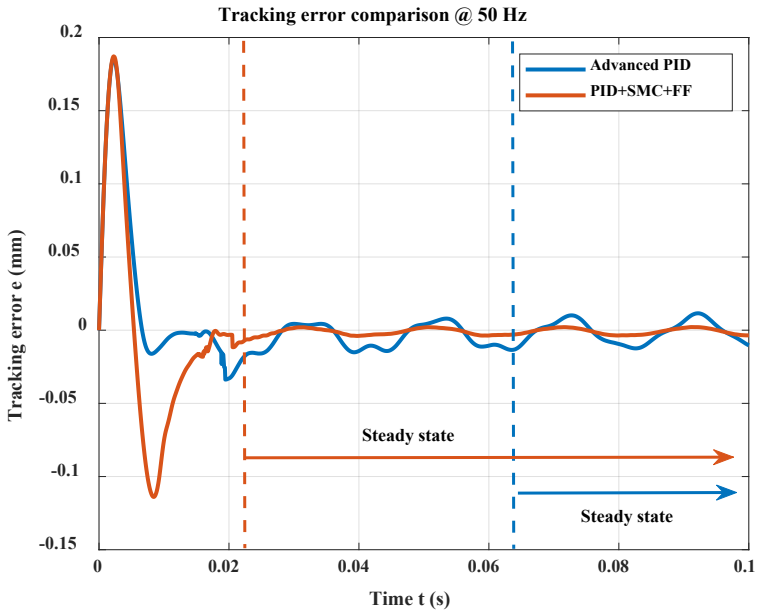

Figure 22 Tracking error comparison results

The values of steady state tracking error of advanced PID and PID+SMC+FF are ±0.012 mm and ±0.003 mm respectively. Also, as shown in Figure 23, the system with the PID+SMC+FF algorithm reaches a steady state after the first period of the input signal (0.0222s), whilst the system with the advanced PID control reaches steady state after three periods of the input signal (0.0640s). This indicates that the PID+SMC+FF algorithm can offer a faster response than advanced PID control.

Table 4 lists the steady state error results under different input signals with advanced PID control and PID+SMC+FF.

Table 4 Steady state tracking error of advanced PID and PID+SMC+FF

Steady state error				
	1.00 mm @ 30 Hz	0.68 mm @ 40 Hz	0.43 mm @ 50 Hz	0.3 mm @ 60 Hz
Advanced PID	1.211%	1.938%	3.135%	5.560%
PID+SMC+FF	0.364%	0.594%	0.871%	1.335%

The steady-state error of the system with PID+SMC+FF is much smaller than that of the system with advanced PID. The higher the input frequency, the more significant are the improvements. In addition to the rapidity and stability of the control system, the bandwidth of

the system can represent the performance of system control. Therefore, the Bode diagrams of the system with different control algorithms are shown in Figure 24.

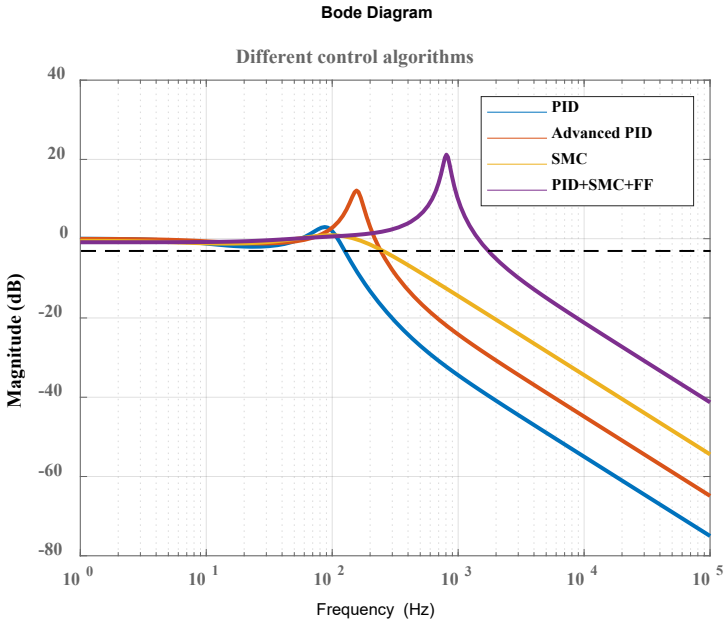

Figure 23 Bode diagram of the system with different control algorithms

Data was obtained from the closed loop frequency sweep of the system. Typically, when the magnitude reaches -3 dB (dashed line), where the output signal is 0.707 times the input signal, the corresponding frequency is defined as the bandwidth of the system. The bandwidths (-3 dB) of the system with different algorithms are listed in Table 5.

Table 5 The bandwidths of the system with different algorithms

	-3 dB (Hz)
PID	125.2
Advanced PID	242.3
SMC	250.3
PID+SMC+FF	1735.0

The PID+SMC+FF algorithm offers the largest bandwidth for the system. Overall, the FTS system with the PID+SMC+FF algorithm gives the best control performance. A compensation method can be implemented to improve the tracking performance further and the final performance can be tested again after compensation.

Given the absence of phase error, amplitude error is the main reason for the tracking error. Using this feature to perform the compensation, Figure 25 shows the compensation steps for the system.

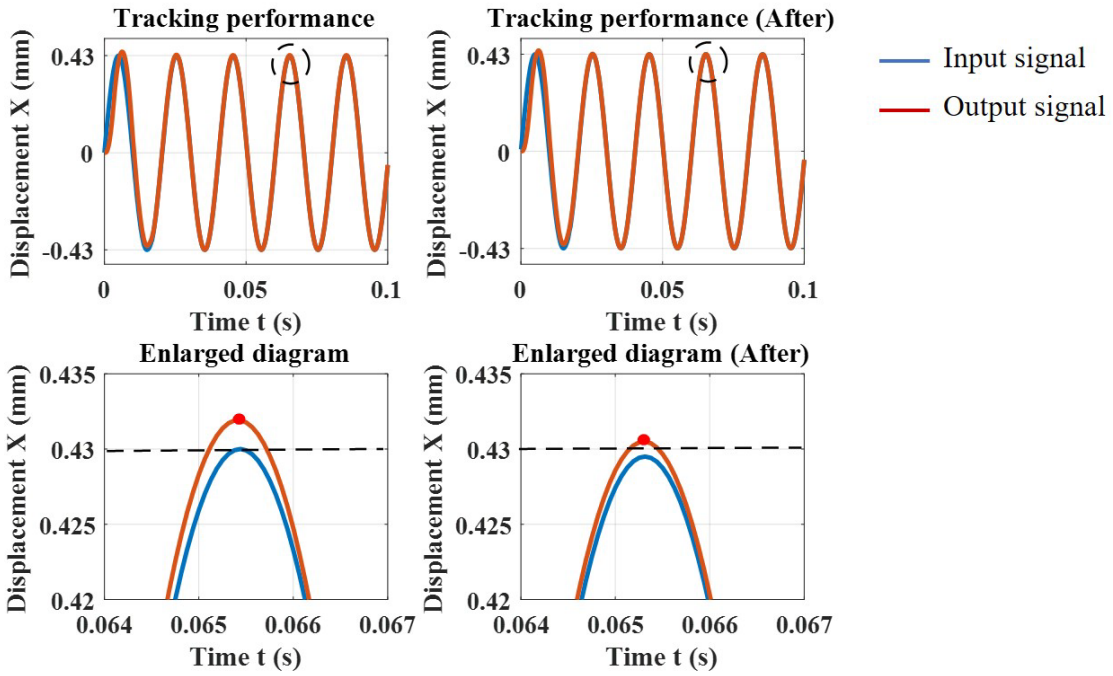

Figure 24 Compensation steps for the system

First, performance in tracking the sine signal (0.43 mm @ 50 Hz) was tested. From the enlarged diagram, it can be observed that the amplitude of the signal is 0.43192 mm with an overshoot of 0.00192mm. If the input signal is decreased to 0.42950mm, the ideal output amplitude is 0.43mm which is the command position at the first place. The test results are shown in the enlarged diagram ('After'), and the amplitude is 0.42950mm which is closer to 0.43mm than before. The same compensation was applied on different input signals, and the results are shown in Table 6.

Table 6 The compensation results of different input signals

Input frequency (Hz)	Input amplitude (mm)	Output amplitude (mm)	ratio	Compensated amplitude (mm)	New output amplitude (mm)	Tracking error
30	1.00000	0.99931	1.001	1.00110	1.00029	0.029%
40	0.68000	0.67999	1.000	0.68110	0.68115	0.169%
50	0.43000	0.43192	0.996	0.42950	0.42967	0.077%
60	0.30000	0.30123	0.996	0.29900	0.30025	0.083%

Essentially, the compensation method is a kind of feed-forward control which can detect system overshoot in advance and realise the compensation on the input signal. This method is suitable for a system with small phase error and where phase error needs to be corrected. The FTS system with the PID+SMC+FF algorithms is suitable for compensation. With the additional help of compensation, the tracking error is reduced to less than 1%, and is controlled

at around 250 nm which satisfies the design requirements. This compensation method is an overshoot correction method for the FTS system when phase difference is absent. This engineering approach is normally applied to the maximum amplitude at each frequency. Before actual machining, the system is tested to determine the compensation ratios at different frequencies, and a lookup table is then generated for the FTS system. This compensation method can be used after the fine-tuning of the system and is the last step of control system tuning.

4.2 Maximum stroke and frequency tests

Tests are performed to determine the capability of the FTS system developed. When the system is run with maximum available stroke of ±3mm at 5Hz, the results show a maximum tracking error of 2.07 μm (Figure 26 (a)), whilst then the system is run with 0.1 mm amplitude at the maximum working frequency of 100 Hz, the results show a maximum tracking error of 3.78 μm (Figure 26 (b)).

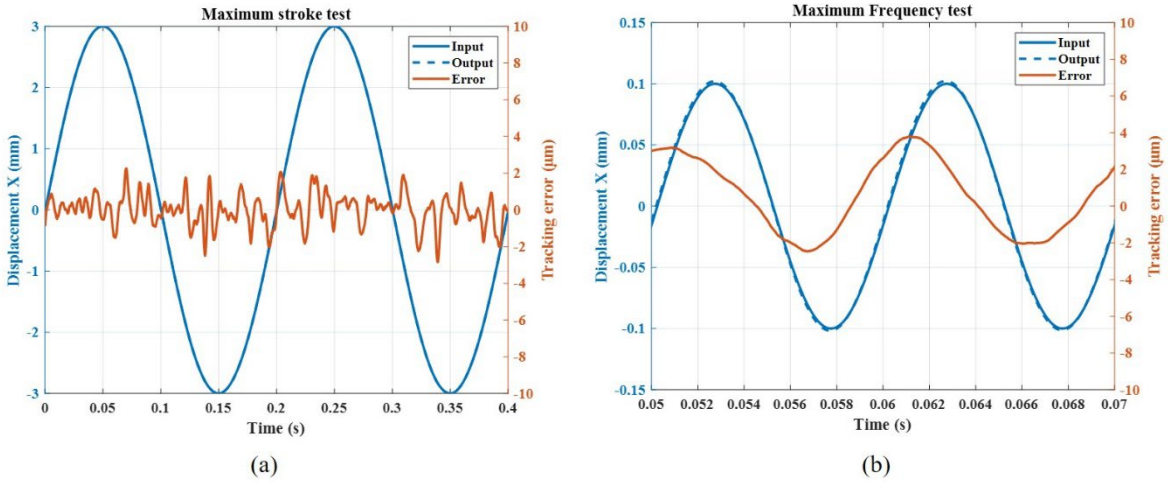

Figure 26 Results of system (a) maximum stroke test and (b) maximum frequency test

5. Conclusions and future work

In this paper, the influence of three traditional control algorithms on an LF-FTS system are compared, and a new hybrid control algorithm is designed and tested. Tracking performance and control characteristics are investigated. The following conclusions can be drawn:

1. Regarding rigidity and stability, PID control and advanced PID with feed-forward control offer short rise times in the system of 0.012 s and 0.014 s respectively.

However, the PID-controlled system exhibits an overshoot. SMC can solve the overshoot problem but the rise time then increases.

2. Considering the accuracy of the control system, PID control can achieve the basic tracking requirements, but the tracking error is unacceptable (75.034% @ 50 Hz). The addition of velocity/acceleration feed-forward control decreases the phase error and results in lower tracking error (3.135% @ 50 Hz). The single-use of SMC can only has a better tracking performance than PID control (11.341% @ 50 Hz).
3. A hybrid control algorithm (PID+SMC+FF) is proposed and tested on the designed LF-FTS. It is a combination of PID control, feed-forward control and the SMC algorithm. A rise time of 0.0134s was measured with no overshoot. The tracking performance increased to less than 1% (0. 871% @ 50 Hz). From frequency domain analysis, the -3dB bandwidth of the control system is increased from hundreds to thousands of Hertz (1735 Hz). PID+SMC+FF is a more appropriate control algorithm for the LF-FTS system.
4. Input signals with different frequencies were tested for the new control algorithm, and the results show that the algorithm is highly suitable for application. Furthermore, due to the complete lack of phase error, a compensation method can be applied which further reduces the system tracking error to 0.029%.

Future work will focus on the performance evaluation of the designed LT-FTS using various control algorithms in machining experiments.

6. References

[1] D. L. Trumper and X. Lu, “Fast Tool Servos: Advances in Precision, Acceleration, and Bandwidth,” *Towar. Synth. Micro-/Nano-systems*, pp. 11–19, 2006, doi: 10.1007/1-84628-559-3_2.

[2] G. Park, M. T. Bement, D. A. Hartman, R. E. Smith, and C. R. Farrar, “The use of active materials for machining processes: A review,” *Int. J. Mach. Tools Manuf.*, vol. 47, no. 15, pp. 2189–2206, 2007, doi: 10.1016/j.ijmachtools.2007.06.002.

[3] Y. Altintas and A. Woronko, “A piezo tool actuator for precision turning of hardened shafts,” *CIRP Ann. - Manuf. Technol.*, vol. 51, no. 1, pp. 303–306, 2002, doi: 10.1016/S0007-8506(07)61522-4.

[4] O. Sosnicki, A. Pages, C. Pacheco, and T. Maillard, “Servo piezo tool SPT400MML for the fast and precise machining of free forms,” *Int. J. Adv. Manuf. Technol.*, vol. 47, no. 9–12, pp. 903–910, 2010, doi: 10.1007/s00170-009-2140-6.

[5] Y. Yang, S. Chen, D. Huo, and K. Cheng, “Performance analysis and optimal design of fast tool servo used for machining microstructured surfaces,” *Proc. Inst. Mech. Eng. Part C J. Mech. Eng. Sci.*, vol. 222, no. 8, pp. 1541–1546, 2008, doi: 10.1243/09544062JMES696.

[6] S. Rakuff and J. F. Cuttino, “Design and testing of a long-range, precision fast tool servo system for diamond turning,” *Precis. Eng.*, vol. 33, no. 1, pp. 18–25, 2009, doi: 10.1016/j.precisioneng.2008.03.001.

[7] M. F. Byl and D. L. Trumper, “A long stroke fast tool servo with integral balance mass,” *Proc. 20th Annu. ASPE Meet. ASPE 2005*, 2005.

[8] F. Tian, Z. Yin, and S. Li, “Fast axis servo for the fast and precise machining of non-rotational symmetric optics,” in *7th International Symposium on Advanced Optical Manufacturing and Testing Technologies: Advanced Optical Manufacturing Technologies*, Aug. 2014, vol. 9281, p. 928103, doi: 10.1117/12.2067863.

[9] L. Zhu, Z. Li, F. Fang, S. Huang, and X. Zhang, “Review on fast tool servo machining of optical freeform surfaces,” *Int. J. Adv. Manuf. Technol.*, vol. 95, no. 5–8, pp. 2071–2092, 2018, doi: 10.1007/s00170-017-1271-4.

[10] X. H. Wang, Z. Ding, and Y. Z. Ma, “Turning of Micro-Structured Surfaces Based on a Fast Tool Servo System,” *Appl. Mech. Mater.*, vol. 684, pp. 308–312, Oct. 2014, doi: 10.4028/www.scientific.net/AMM.684.308.

[11] X. Lu, “Electromagnetically-Driven Ultra-Fast Tool Servos for Diamond Turning,” *CIRP Ann. - Manuf. Technol.*, no. 1997, p. 351, 2005.

[12] H. Wang and S. Yang, “Design and control of a fast tool servo used in noncircular piston turning process,” *Mech. Syst. Signal Process.*, vol. 36, no. 1, pp. 87–94, 2013, doi: 10.1016/j.ymssp.2011.07.013.

[13] H. Ma, J. Tian, and D. Hu, “Development of a fast tool servo in noncircular turning and its control,” *Mech. Syst. Signal Process.*, vol. 41, no. 1–2, pp. 705–713, 2013, doi: 10.1016/j.ymssp.2013.08.011.

[14] X. Zhou, Z. Zhu, S. Zhao, J. Lin, and J. Dou, “An improved adaptive feedforward cancellation for trajectory tracking of fast tool servo based on fractional calculus,” *Procedia Eng.*, vol. 15, pp. 315–320, 2011, doi: 10.1016/j.proeng.2011.08.061.

[15] J. Li, X. Qi, Y. Xia, F. Pu, and K. Chang, “Frequency domain stability analysis of nonlinear active disturbance rejection control system,” *ISA Trans.*, vol. 56, pp. 188–195, 2015, doi: 10.1016/j.isatra.2014.11.009.

[16] D. Wu, K. Chen, and X. Wang, “Tracking control and active disturbance rejection with application to noncircular machining,” *Int. J. Mach. Tools Manuf.*, vol. 47, no. 15, pp. 2207–2217, 2007, doi: 10.1016/j.ijmachtools.2007.07.002.

[17] C. Y. Lin and P. Y. Chen, “Precision tracking control of a biaxial piezo stage using repetitive

control and double-feedforward compensation," *Mechatronics*, vol. 21, no. 1, pp. 239–249, 2011, doi: 10.1016/j.mechatronics.2010.11.002.

[18] F. Duan, W. Le Zhu, A. Sun, and B. F. Ju, "Systematic modeling and rapid control for diamond machining of periodical optical surface," *J. Manuf. Process.*, vol. 56, no. May, pp. 451–462, 2020, doi: 10.1016/j.jmapro.2020.05.003.

[19] J. E. Azzaro and R. A. Veiga, "Sliding Mode Controller with Neural Network Identification," *IEEE Lat. Am. Trans.*, vol. 13, no. 12, pp. 3754–3757, Dec. 2015, doi: 10.1109/TLA.2015.7404904.

[20] H. Zhang, G. Dong, M. Zhou, C. Song, Y. Huang, and K. Du, "A new variable structure sliding mode control strategy for fts in diamond-cutting microstructured surfaces," *Int. J. Adv. Manuf. Technol.*, vol. 65, no. 5–8, pp. 1177–1184, 2013, doi: 10.1007/s00170-012-4249-2.